Annals of Nuclear Medicine Vol. 19, No. 7, 617–625, 2005

Radiosynthesis and *in vivo* evaluation of ^{11}C-labeled 1,5-diarylpyrazole derivatives for mapping cyclooxygenases

Yoshihiko FUJISAKI,* Kazunori KAWAMURA,** Wei-Fang WANG,** Kiichi ISHIWATA,** Fumihiko YAMAMOTO,* Takashi KUWANO,*** Mayumi ONO*** and Minoru MAEDA*

**Graduate School of Pharmaceutical Sciences and ***Graduate School of Medical Sciences, Kyushu University*
***Positron Medical Center, Tokyo Metropolitan Institute of Gerontology*

We prepared ^{11}C-labeled 5-(4-chlorophenyl)-1-(4-methoxyphenyl)-3-(trifluoromethyl)-1*H*-pyrazole ([^{11}C]**1**) and 4-[5-(4-methoxyphenyl)-3-trifluoromethyl-1*H*-pyrazol-1-yl]benzenesulfonamide ([^{11}C]**2**) for imaging COX-1 and COX-2 isoforms, respectively, by positron emission tomography. [^{11}C]**1** and [^{11}C]**2** were synthesized in high radiochemical yields by *O*-[^{11}C]methylation with [^{11}C]methyl triflate in acetone containing an equivalent of NaOH as a base with respect to the phenolic precursors. *In vivo* evaluation in rats bearing AH109A hepatoma demonstrated minimal specific binding of [^{11}C]**1** to COX-1 in peripheral organs, such as the spleen and small intestine. Carrier-saturable uptake of [^{11}C]**2** was found in the spleen, but COX-2-specific binding of [^{11}C]**2** was not identifiable in the brain, AH109A hepatoma or other peripheral organs, although *ex vivo* autoradiography showed regionally different distribution in the brain and AH109A. The results suggest that neither [^{11}C]**1** nor [^{11}C]**2** is a suitable radioligand for *in vivo* biomarkers of COX enzymes, mainly because of marked non-specific binding.

Key words: cyclooxygenase inhibitor, carbon-11, radiosynthesis, tissue distribution

INTRODUCTION

CYCLOOXYGENASE (COX), also represented as prostaglandin H synthase, is one of the key enzymes in converting arachidonic acid into prostanoids such as prostaglandins and thromboxanes.[1] After the discovery of two distinct isoforms of the cyclooxygenase,[2–5] COX-1 and COX-2, it was demonstrated that non-steroidal anti-inflammatory drugs (NSAIDs) exert their effects by inhibiting COX-2, an inducible form that is initiated by diverse inflammatory stimuli, oncoproteins and growth factors.[6] Moreover, it has been shown that the side effects of NSAIDs, such as gastrointestinal ulceration and bleeding, are ascribable to a suppression of COX-1 that is constitutively expressed in most tissues and acts as a housekeeping enzyme. Therefore, a number of COX-2 selective inhibitors have been identified as new NSAIDs.[7–9]

It has been shown that induction of COX-2 is found in not only inflammation but also some other pathological processes. For example, COX-2 is up-regulated in various tumors, including colon,[10–12] lung,[13,14] and breast cancer,[15] and associated with metastatic tumor behavior. Thus, the specific expression of COX-2 in tumors but not in normal tissue may serve as a potential target for anticancer therapy.[16,17] Besides, it has also been suggested that COX-2 induction is associated with cerebrovascular and neurodegenerative diseases such as Alzheimer's and Parkinson's diseases.[18,19] In addition, it is known that COX-2 is constitutively expressed at relatively high levels in the brain and to a lesser extent in the kidney, heart and lung.[20,21] Accordingly, this isoform is thought to play specific roles physiologically and pathologically.

On the other hand, COX-1 is expressed primarily in normal tissues and produces prostaglandins that regulate rapid physiological responses.[20] In the brain COX-1 is most abundant in the forebrain, where the prostaglandins may be involved in the control of the autonomic nervous

Received March 22, 2005, revision accepted July 7, 2005.

For reprint contact: Minoru Maeda, Ph.D., Graduate School of Pharmaceutical Sciences, Kyushu University, 3–1–1 Maidashi, Higashi-ku, Fukuoka 812–8582, JAPAN.

E-mail: maeda@phar.kyushu-u.ac.jp

system and sensory processing.[22] Interestingly, COX-1 mRNA is rapidly induced in the cerebral cortex in a rat model of reversible ischemia.[23]

Our purpose in this study is the development of positron-emitting isozyme-selective COX inhibitors that would give images of COX-1 and COX-2 enzyme distribution by positron emission tomography (PET). This noninvasive method may serve as a novel imaging tool for *in vivo* study of enzyme molecules, as well as for predictive evaluation of COX-targeted therapy. Many compounds with a central heterocyclic core having two vicinal aryl rings have been studied extensively for selective cyclooxygenase inhibition since the discovery of celecoxib[24] and rofecoxib[25] as promising lead structures for selective COX-2 inhibition. So far three positron-emitting COX inhibitors, [^{18}F]SC63217 (COX-1 $IC_{50} < 10$ nM; COX-2 $IC_{50} > 100$ μM),[26] [^{18}F]SC58125 (COX-1 $IC_{50} > 100$ μM; COX-2 $IC_{50} < 86$ nM),[26] and [^{18}F]desbromo-DuP-697 (COX-1 $IC_{50} > 100$ μM; COX-2 $IC_{50} = 250$ nM)[27,28] have been prepared and evaluated, but no promising radiotracers for COX imaging in either the brain or peripheral regions have been found up to the present.

We chose two 1,5-diarylpyrazole derivatives as COX inhibitors for labeling with ^{11}C (Fig. 1): 5-(4-chlorophenyl)-1-(4-methoxyphenyl)-3-(trifluoromethyl)-1*H*-pyrazole (**1**), a selective COX-1 inhibitor (COX-1 IC_{50} = 9 nM; COX-2 IC_{50} = 6.3 μM),[29] and 4-[5-(4-methoxyphenyl)-3-trifluoromethyl-1*H*-pyrazol-1-yl]benzenesulfonamide (**2**), a selective COX-2 inhibitor (COX-1 IC_{50} = 2.6 μM; COX-2 IC_{50} = 8 nM).[24] These compounds were previously reported to be potent and selective COX inhibitors, which differ structurally in their substituents only on the phenyl ring. Compound **1** has been used in many pharmacological and toxicological studies as a COX-1 inhibitor.[29,30] Moreover, these inhibitors structurally have a methoxy group on the benzene ring and therefore are suitable for labeling with ^{11}C. These observations prompted us to synthesize ^{11}C-labeled analogs, and to characterize their *in vivo* behavior. In this paper, we describe the radiolabeling of both COX inhibitors (**1** and **2**) with ^{11}C and their *in vivo* evaluation using tumor-bearing rats.

MATERIALS AND METHODS

The reference compounds, 5-(4-chlorophenyl)-1-(4-methoxyphenyl)-3-(trifluoromethyl)-1*H*-pyrazole (**1**) and 4-[5-(4-methoxyphenyl)-3-trifluoromethyl-1*H*-pyrazol-1-yl]benzenesulfonamide (**2**) were prepared according to the published method.[24] Indomethacin and NS-398 were purchased from Sigma-Aldrich Inc. (St. Louis, MO). All chemicals and solvents were obtained from commercial sources. Male Donryu rats (7 weeks old) were obtained from Tokyo Laboratory Animals Co., Ltd. (Tokyo, Japan). AH109A ascitic hepatoma cells were subcutaneously inoculated on the back of Donryu rats,[31] which were used for the following experiments 7–10 days after inoculation. The animal studies were approved by the Animal Care and Use Committee of the Tokyo Metropolitan Institute of Gerontology. ^{1}H-NMR spectra were measured on a Varian UNITY-400 spectrometer with tetramethylsilane as the internal standard, using dimethyl sulfoxide-d_6 as the solvent. All chemical shifts (δ) are reported in parts per million (ppm) downfield from the standard. Infrared (IR) spectra were recorded with a SHIMADZU FTIR-8400 spectrometer. Mass spectra were obtained on an Applied Biosystems Mariner System 5299 spectrometer. Melting points were determined on a Yanagimoto melting point apparatus. Column chromatography was done on Merck Kieselgel 60 (70–230 mesh).

1. Preparation of labeling precursors

*5-(4-Chlorophenyl)-1-(4-hydroxyphenyl)-3-(trifluoromethyl)-1H-pyrazole (**3**)*

5-(4-Chlorophenyl)-1-(4-methoxyphenyl)-3-(trifluoromethyl)-1*H*-pyrazole (**1**) was prepared as previously reported.[24] BBr_3 (1 M in CH_2Cl_2, 10 m*l*, 10 mmol) was added dropwise to an ice-cooled solution of **1** (1.2 g, 3.35 mmol) in CH_2Cl_2 (25 m*l*). The mixture was stirred at 5°C for 2 hours, poured into ice-H_2O, extracted with EtOAc, and concentrated *in vacuo*. The residue was chromatographed on a silica gel with hexane : EtOAc = 5 : 1 to provide the desired compound **3** (877.6 mg, 77.5%) as a white solid: m.p. 180–183°C; ^{1}H-NMR (DMSO-d_6) δ: 6.79 (d, J = 8.79 Hz, 3H), 7.15 (d, J = 8.61 Hz, 2H), 7.17 (s, 1H), 7.28 (d, J = 8.42 Hz, 2H), 7.44 (d, J = 8.43 Hz, 2H), 9.94 (s, 1H); FTIR (KBr) cm^{-1}: 3258; ESIMS (m/z): 339 $(M + H)^+$.

*4-[5-(4-Hydroxyphenyl)-3-trifluoromethyl-1H-pyrazol-1-yl]benzenesulfonamide (**4**)*

4-[5-(4-Methoxyphenyl)-3-trifluoromethyl-1*H*-pyrazol-1-yl]benzenesulfonamide (**2**) was prepared as previously reported.[24] BBr_3 (1 M in CH_2Cl_2, 1.1 m*l*, 1.1 mmol) was added dropwise to an ice-cooled solution of **2** (104.3 mg, 262.5 μmol) in CH_2Cl_2 (4 m*l*). The mixture was stirred at 5°C for 2 hours, poured into ice-H_2O, extracted with EtOAc, and concentrated *in vacuo*. The residue was chromatographed on a silica gel with $CHCl_3$: acetone = 8 : 1 to give **4** (27.7 mg, 40.8%) as a pale yellow solid: m.p. 213–216°C; ^{1}H-NMR (DMSO-d_6) δ: 6.76 (d, J = 8.79 Hz, 2H), 7.08 (s, 1H), 7.10 (d, J = 8.61 Hz), 7.49 (s, 2H), 7.52 (d, J = 8.79 Hz), 7.86 (d, J = 8.80 Hz), 9.88 (s, 1H); FTIR (KBr) cm^{-1}: 3290; ESIMS (m/z): 384 $(M + H)^+$.

2. Preparation of radiolabeled compounds

*[O-Methyl-^{11}C]-5-(4-chlorophenyl)-1-(4-methoxyphenyl)-3-(trifluoromethyl)-1H-pyrazole ([^{11}C]**1**)*

[^{11}C]**1** was synthesized by [^{11}C]methylation of **3** with [^{11}C]methyl iodide or [^{11}C]methyl triflate prepared using an automated synthesis system as previously described.[32,33] [^{11}C]Methyl iodide or [^{11}C]methyl triflate was trapped in

250 μl of solvent (DMF or acetone) containing 0.25 mg (0.7 μmol) of **3** and 1 mg (40 μmol) of NaH as a base for [^{11}C]CH_3I, or 5 μl (5 μmol) of 1.0 M aqueous NaOH or 5 μl (0.7 μmol) of 1/7 M aqueous NaOH as a base for [^{11}C]CH_3OTf. The reaction vessel was heated at 120°C for 1 minute when DMF was used as the solvent. When acetone was used, the reaction was carried out at room temperature for 2 minutes. After 1.3 m*l* of 0.1 M HCl/CH_3CN/H_2O (10/9/1, v/v/v) had been added, the reaction mixture was applied to high performance liquid chromatography (HPLC) using a reversed phase column (YMC-Pack ODS-A, 10 mm inner diameter × 250 mm length, YMC Co., Ltd., Kyoto, Japan), comprising a UV absorbance (260 nm) with an NaI (Tl) scintillation detector. The mobile phase was a mixture of CH_3CN and H_2O (9/1, v/v) at a flow rate of 6 m*l*/minute. The [^{11}C]**1** fraction (retention time: 4.5–5.0 minutes for [^{11}C]**1** and 3.5–4.0 minutes for **3**) was collected and evaporated to dryness. The residue was dissolved in physiological saline containing 0.125% Tween 80, and filtered through a 0.22 mm membrane. The labeled compound was analyzed by HPLC: column, TSKgel Super-ODS (4.6 mm inner diameter × 100 mm length, Toso Co., Ltd., Tokyo, Japan); mobile phase, CH_3CN/H_2O (7/3, v/v); flow rate, 1.0 m*l*/minute; and retention time: 4.3 minutes for [^{11}C]**1**. The specific activity at the end of synthesis calculated by UV spectroscopy (at 260 nm) was in the range of 71–125 GBq/μmol.

*4-[5-(4-([^{11}C]Methoxyphenyl)-3-trifluoromethyl-1H-pyrazol-1-yl)benzenesulfonamide ([^{11}C]**2**)*

[^{11}C]**2** was prepared by a method similar to that for [^{11}C]**1** with a slight modification in the HPLC separation, except that **4** (0.25 mg, 0.68 μmol) was used as the precursor. At the end of the reaction, 1.3 m*l* of 0.1 M HCl/CH_3CN/H_2O (5/3/2, v/v/v) was added, and the reaction mixture was applied to HPLC using the same reversed phase column. The mobile phase was a mixture of CH_3CN and H_2O (6/4, v/v) at a flow rate of 5 m*l*/minute and the retention times were 8.5–9.0 minutes for [^{11}C]**2** and 5.0–5.5 minutes for **4**. Then the [^{11}C]**2** fraction prepared for injection was analyzed by the same HPLC with a different mobile phase of CH_3CN/H_2O (5/5, v/v): retention time, 5.0 minutes for [^{11}C]**2**. The specific activity at the end of synthesis was calculated by UV spectroscopy (at 260 nm) to be in the range of 27–61 GBq/μmol.

Octanol-water partition coefficient

[^{11}C]**1** (3.5 MBq) or [^{11}C]**2** (1.8 MBq) in a mixture of 2 m*l* of octanol and 2 m*l* of phosphate-buffered saline (PBS) was incubated for 30 minutes at 37°C in a water bath. After the layers had been separated, 0.1 m*l* of the organic layer and 0.8 m*l* of the aqueous layer were taken and then the samples of the two phases were counted with an auto-γ-counter (LKB Wallac Compugamma 1282CS, Turku, Finland). In six independent measurements, the average octanol-water partition coefficients were expressed as $\log P_{7.4}$.

3. Animal studies

Tissue distribution of the tracers in rats

Each tracer was intravenously injected into rats bearing the AH109A hepatoma. They were killed by cervical dislocation 5, 15, 30, and 60 minutes after injection (n = 4–5). The body weight of the rats was 279 ± 56 g. The injected doses of the tracers were 10 MBq/0.15 or 0.23 nmol. The blood was collected by heart puncture and the tissues were harvested. The ^{11}C in the samples was counted with an auto-γ-counter and weighed. The tissue uptake of ^{11}C was expressed as a percentage of injected dose per gram of tissue (%ID/g).

In the other group of rats, a blocking experiment to determine the COX-specific uptake of the tracers was carried out. Each tracer (10 MBq/0.23 or 0.90 nmol) was co-injected with each of the following blockers: unlabeled **1** and **2**, indomethacin (non-selective COX inhibitor, COX-1 IC_{50} = 100 nM; COX-2 IC_{50} = 900 nM)[34] or NS-398 (COX-2 selective inhibitor, COX-1 IC_{50} > 100 μM; COX-2 IC_{50} = 100 nM).[34] Each blocker was dissolved in dimethyl sulfoxide, and the co-injected dose was 1 mg/kg. In the control rats the same amount of dimethyl sulfoxide was co-injected. Thirty minutes later the rats were killed (n = 4–5), and the tissue uptake of ^{11}C was expressed as %ID/g.

Metabolite analysis

[^{11}C]**1** or [^{11}C]**2** (210–215 MBq/2.2–7.7 nmol) was intravenously injected into rats bearing the AH109A hepatoma, and 30 minutes later they were killed by cervical dislocation (n = 3). The blood was removed by heart puncture using a heparinized syringe, and the brain and AH109A were removed. The blood was centrifuged at 7,000 × *g* for 1 minute at 4°C to obtain plasma, which was denatured with 1/3 equivalent volume of 20% trichloroacetic acid (TCA) in CH_3CN. The mixture was centrifuged under the same conditions, and the precipitate was re-suspended in 1 m*l* of 10% TCA in CH_3CN, followed by centrifugation. This procedure was repeated three times. The brain and AH109A (approximately 200 mg) were homogenized in 0.5 m*l* of 20% TCA in CH_3CN. The homogenate was then treated as described above. The combined supernatant was analyzed by HPLC with a radioactivity detector (FLO-ONE/Beta A200, Packard, Meriden, CT). A Radial-Pak C18 column equipped with an RCM 8 × 10 module (8 mm × 100 mm, Waters, Milford, MA) was used with a mixture of CH_3CN and 50 mM sodium acetate buffer (pH 6.0) (7/3 for [^{11}C]**1**, and 45/55 for [^{11}C]**2**, v/v) as the mobile phase at a flow rate of 2 m*l*/minute.

Ex vivo autoradiographic studies in rats

Each tracer was intravenously injected into two rats bearing the AH109A hepatoma. One rat was a control and the other was treated with an intravenous injection of a

COX inhibitor (1 mg/kg): indomethacin for [^{11}C]**1** and NS-398 for [^{11}C]**2**, 5 minutes prior to the tracer injection. The rats were killed by cervical dislocation 30 minutes after the tracer injection. The brain was rapidly dissected and the right hemisphere of the control and the left hemisphere of the rat given the blocker were put side by side for comparison. In two other rats, the AH109A tissue was dissected 30 minutes after intravenous injection of [^{11}C]**1** or [^{11}C]**2**. The injected doses of the tracers were 170–200 MBq/2.5–14 nmol. The hybrid brain and AH109A tissues were frozen and cut into 30 μm-thickness using a cryotome (Bright Instrument Co., Ltd., Huntingdon, UK). The brain and AH109A sections were dried on a hot plate at 60°C and apposed on a storage phosphor screen (Phosphor Imager SI System, Molecular Dynamics, Sunnyvale, CA), and the distribution was visualized.

Western blot analysis

Western blot analysis was performed as described previously to determine whether AH109A tumor cells expressed the COX-2 isoform.[35] KB3-1 cells (head and neck cancer cell, positive control), AH109A cells or ascites of AH109A bearing Donryu rat, in medium containing 0.5% fetal bovine serum, were incubated for 24 hr at 37°C in the absence or presence of 1 ng/m*l* IL-1β. The cells were then rinsed with ice-cold PBS and lysed in Triton X-100 buffer (50 mM HEPES, 150 mM NaCl, 1% Triton X-100, and 10% glycerol containing 1 mM phenylmethylsulfonyl fluoride, 10 μg/m*l* aprotinin, 10 μg/m*l* leupeptin, and 1 mM sodium vanadate). Ascites of AH109A bearing Donryu rat were sonicated and then protein was extracted. Proteins were subjected to SDS-PAGE and transferred to a polyvinylidene difluoride membrane. After transfer, blots were incubated for 2 hr at room temperature with the blocking solution and probed with anti COX-2 antibody (Santa Cruz Biotechnology, San Diego), followed by washing. The protein content was visualized using horseradish-conjugated secondary antibodies, followed by enhanced chemiluminescence (Amersham, Piscatawaym NJ).

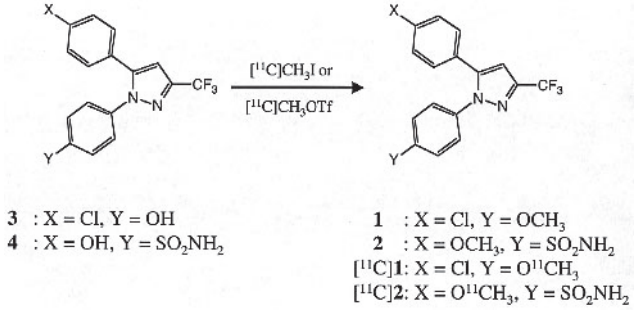

Fig. 1 Chemical structures of ^{11}C-labeled/unlabeled COX inhibitors and radiosynthesis by *O*-[^{11}C]methylation.

RESULTS

Radiochemistry

COX inhibitors **1** and **2** have in their structure one aromatic methoxy group which provides easy access to ^{11}C-labeling by *O*-methylation of the corresponding desmethyl compound with either [^{11}C]methyl iodide or [^{11}C]methyl triflate. Therefore, the desmethyl precursors, **3** and **4** for carbon-11 labeling, were prepared by demethylation of **1** and **2**, which were prepared according to the published method,[24] with boron tribromide. Precursors **3** and **4** were characterized by the appearance of a peak ~9.9 ppm in the ^{1}H-NMR spectra, which were assigned as being due to the phenolic OH.

Initial attempts to react the two precursors **3** and **4** with [^{11}C]methyl iodide in DMF using NaH as a base, employing the standard conditions (120°C, 1 min) that have so far been used in our laboratory, yielded radiochemical yields of 20–40% for [^{11}C]**1** and 20–22% for [^{11}C]**2**, respectively. Recently it has been demonstrated that [^{11}C]methyl triflate is a highly reactive alternative to [^{11}C]methyl iodide as a labeling agent, which offers several advan-

Table 1 Radiosynthesis of [^{11}C]**1** and [^{11}C]**2**

	Agent	Solvent	Base		Radiochemical yield (%)[a]
[^{11}C]**1**	[^{11}C]CH_3I	DMF[b]	40–80 μmol	NaH	29.0 (range, 19.9–40.0, n = 3)
	[^{11}C]CH_3OTf	DMF[c]	5 μmol	NaOH	7.3 (n = 1)
		DMF[c]	0.7 μmol	NaOH	21.6 (n = 1)
		Acetone[c]	0.7 μmol	NaOH	74.5 (n = 1)
		Acetone[c]	none		< 0.1 (n = 1)
[^{11}C]**2**	[^{11}C]CH_3I	DMF[b]	40–80 μmol	NaH	21.5 (range, 20.6–22.2, n = 3)
	[^{11}C]CH_3OTf	DMF[c]	5 μmol	NaOH	11.8 (n = 1)
		Acetone[c]	5 μmol	NaOH	5.4 (n = 1)
		Acetone[c]	0.7 μmol	NaOH	46.6 (range, 44.3–48.9, n = 2)

[a]Decay-corrected radiochemical yields based on [^{11}C]methyl iodide or [^{11}C]methyl triflate.
[b][^{11}C]Methyl iodide was trapped in the solvent at −12°C and the reaction mixture was heated at 120°C for 1 minute.
[c][^{11}C]Methyl triflate was trapped in the solvent at room temperature for 2 minutes.

Table 2 Tissue distribution of radioactivity after intravenous injection of [^{11}C]**1** into AH109A hepatoma bearing rats

	Uptake (%ID/g)*			
	5 min	15 min	30 min	60 min
Blood	0.18 ± 0.03	0.12 ± 0.02	0.12 ± 0.01	0.11 ± 0.02
Brain	0.42 ± 0.05	0.29 ± 0.02	0.25 ± 0.02	0.14 ± 0.02
Heart	0.94 ± 0.11	0.32 ± 0.03	0.25 ± 0.02	0.16 ± 0.03
Lung	0.98 ± 0.28	0.49 ± 0.06	0.43 ± 0.04	0.34 ± 0.04
Liver	1.30 ± 0.20	0.86 ± 0.14	0.84 ± 0.23	0.72 ± 0.21
Spleen	0.62 ± 0.11	0.51 ± 0.07	0.40 ± 0.03	0.24 ± 0.03
Pancreas	0.71 ± 0.03	0.42 ± 0.09	0.37 ± 0.06	0.44 ± 0.11
Small intestine	0.59 ± 0.11	0.49 ± 0.05	0.40 ± 0.04	0.32 ± 0.08
Kidney	0.83 ± 0.12	0.40 ± 0.02	0.32 ± 0.04	0.29 ± 0.03
Muscle	0.39 ± 0.08	0.24 ± 0.04	0.16 ± 0.02	0.13 ± 0.01
AH109A	0.19 ± 0.04	0.23 ± 0.04	0.20 ± 0.03	0.20 ± 0.01

*Mean ± S.D. (n = 4).

Table 3 Tissue distribution of radioactivity after intravenous injection of [^{11}C]**2** into AH109A hepatoma bearing rats

	Uptake (%ID/g)*			
	5 min	15 min	30 min	60 min
Blood	1.38 ± 0.05	1.15 ± 0.08	0.99 ± 0.11	1.02 ± 0.03
Brain	0.17 ± 0.01	0.20 ± 0.01	0.19 ± 0.01	0.20 ± 0.02
Heart	0.68 ± 0.01	0.55 ± 0.05	0.47 ± 0.02	0.47 ± 0.03
Lung	0.74 ± 0.05	0.59 ± 0.06	0.57 ± 0.10	0.51 ± 0.06
Liver	1.48 ± 0.14	1.22 ± 0.09	1.15 ± 0.06	1.09 ± 0.09
Spleen	0.63 ± 0.11	0.68 ± 0.08	0.68 ± 0.16	0.63 ± 0.22
Pancreas	0.70 ± 0.03	0.66 ± 0.04	0.66 ± 0.23	0.55 ± 0.07
Small intestine	0.43 ± 0.03	0.48 ± 0.04	0.42 ± 0.04	0.39 ± 0.02
Kidney	0.72 ± 0.06	0.60 ± 0.03	0.51 ± 0.03	0.52 ± 0.02
Muscle	0.26 ± 0.08	0.24 ± 0.04	0.20 ± 0.00	0.20 ± 0.01
AH109A	0.25 ± 0.02	0.29 ± 0.01	0.25 ± 0.03	0.31 ± 0.04

*Mean ± S.D. (n = 4).

tages.[36] Reactions of **3** and **4** with [^{11}C]methyl triflate in acetone or DMF using NaOH as a base were investigated in the attempt to increase the radiochemical yield. [^{11}C]Methylation reactions using [^{11}C]methyl triflate in acetone or DMF, when a large molar excess of aqueous NaOH relative to the phenolic precursors were present in the reactions, gave lower radiochemical yields. However, the reduction of the amount of NaOH as the base led to a large increase in the radiochemical yields. We found that the use of excess base was not necessary for [^{11}C]methylation of these two precursors to proceed, and the reaction with [^{11}C]methyl triflate only without any base afforded traces of [^{11}C]**1**. Thus, it was concluded that [^{11}C]**1** and [^{11}C]**2** were efficiently prepared by using [^{11}C]methyl triflate as the labeling agent and 0.25 mg of the precursor at room temperature for about 2 min in acetone (0.25 m*l*) containing an equimolar amount of aqueous NaOH with respect to the phenolic precursor. These conditions led to radiochemical yields of 74.5% for [^{11}C]**1** and 46.6% for [^{11}C]**2**, respectively. The total preparation time for both tracers, including purification and formulation, was approximately 20 min from the end of bombardment. The radiochemical purities of both tracers were found to be over 99% while the specific activities at the end of synthesis were in the range of 71–125 GBq/μmol for [^{11}C]**1** and 27–61 GBq/μmol for [^{11}C]**2**. The absence of any residual traces of the starting precursors and other non-radioactive impurities was verified by HPLC analysis. The lipophilicities of the two tracers were evaluated as $\log P_{7.4}$. [^{11}C]**1** ($\log P_{7.4}$ = 3.46) was more lipophilic than [^{11}C]**2** ($\log P_{7.4}$ = 3.06).

Tissue distribution study

The tissue distribution of the radioactivity after injection of each of the two tracers into the rats is summarized in Tables 2 and 3. [^{11}C]**1** showed a rapid blood clearance and the radioactivity levels of the blood were lower than those in all tissues investigated. The radioactivity levels in AH109A slightly increased for the first 15 min and then remained constant, while the radioactivity in other tissues

Table 4 Effects of co-injection of the COX inhibitors on the tissue distribution of radioactivity 30 minutes after intravenous injection of [^{11}C]**1** into AH109A hepatoma bearing rats

	Uptake (%ID/g)*			
	Control	**1**	Indomethacin	**2**
Blood	0.13 ± 0.02	0.13 ± 0.01	0.12 ± 0.02	0.10 ± 0.03
Brain	0.27 ± 0.06	0.29 ± 0.02	0.29 ± 0.04	0.21 ± 0.06
Heart	0.29 ± 0.06	0.30 ± 0.01	0.28 ± 0.05	0.23 ± 0.06
Lung	0.45 ± 0.11	0.33 ± 0.04$^{\#}$	0.38 ± 0.07	0.32 ± 0.10
Liver	1.02 ± 0.13	0.88 ± 0.08	0.80 ± 0.11$^{\#}$	0.79 ± 0.26
Spleen	0.46 ± 0.09	0.20 ± 0.04$^{\#}$	0.21 ± 0.03$^{\#}$	0.32 ± 0.07$^{\#}$
Pancreas	0.49 ± 0.09	0.48 ± 0.06	0.45 ± 0.08	0.37 ± 0.10
Small intestine	0.46 ± 0.08	0.30 ± 0.02$^{\#}$	0.31 ± 0.04$^{\#}$	0.36 ± 0.12
Kidney	0.36 ± 0.07	0.31 ± 0.02	0.31 ± 0.03	0.29 ± 0.09
Muscle	0.22 ± 0.05	0.24 ± 0.01	0.23 ± 0.06	0.17 ± 0.05
AH109A	0.27 ± 0.06	0.25 ± 0.01	0.23 ± 0.03	0.20 ± 0.08

*Mean ± S.D. (n = 4–5).

$^{\#}$Significant decrease ($p < 0.05$) compared to the control (Students t-test).

Table 5 Effects of co-injection of the COX inhibitors on the tissue distribution of radioactivity 30 minutes after intravenous injection of [^{11}C]**2** into AH109A hepatoma bearing rats

	Uptake (%ID/g)*				
	Control	**2**	NS-398	Indomethacin	**1**
Blood	1.10 ± 0.08	0.61 ± 0.12$^{\#}$	1.19 ± 0.23	1.17 ± 0.23	1.23 ± 0.21
Brain	0.23 ± 0.02	0.24 ± 0.03	0.23 ± 0.02	0.23 ± 0.02	0.24 ± 0.03
Heart	0.40 ± 0.08	0.37 ± 0.11	0.54 ± 0.05$^{\$}$	0.57 ± 0.03$^{\$}$	0.56 ± 0.08$^{\$}$
Lung	0.47 ± 0.14	0.48 ± 0.03	0.57 ± 0.14	0.57 ± 0.08	0.62 ± 0.11
Liver	1.21 ± 0.09	1.38 ± 0.15	1.28 ± 0.09	1.24 ± 0.15	1.36 ± 0.21
Spleen	0.73 ± 0.04	0.53 ± 0.08$^{\#}$	0.73 ± 0.09	0.74 ± 0.09	0.68 ± 0.05
Pancreas	0.61 ± 0.05	0.76 ± 0.13$^{\$}$	0.66 ± 0.06	0.65 ± 0.06	0.72 ± 0.13
Small intestine	0.42 ± 0.05	0.51 ± 0.08	0.45 ± 0.04	0.44 ± 0.03	0.48 ± 0.07
Kidney	0.55 ± 0.04	0.63 ± 0.08	0.59 ± 0.03	0.61 ± 0.05	0.66 ± 0.12
Muscle	0.23 ± 0.08	0.30 ± 0.05$^{\$}$	0.24 ± 0.01	0.24 ± 0.01	0.26 ± 0.03$^{\$}$
AH109A	0.35 ± 0.03	0.38 ± 0.05	0.36 ± 0.02	0.36 ± 0.04	0.36 ± 0.05

*Mean ± S.D. (n = 5).

$^{\#}$Significant decrease ($p < 0.05$) and $^{\$}$significant increase ($p < 0.05$) compared to the control (Students t-test).

investigated gradually decreased. Among them, the uptake was relatively retained in the liver, pancreas and small intestine over 60 min after injection.

In contrast to [^{11}C]**1**, the blood clearance of [^{11}C]**2** was much slower (Table 3). The radioactivity levels of the blood were higher than those in all tissues investigated except for the liver. The uptake in the brain and AH109A slightly increased for the first 15 min and then remained constant. The brain uptake was lowest (ca 0.2%ID/g), indicative of poor blood brain barrier penetration. The uptake was relatively retained in the spleen, small intestine and muscle tissue, while the uptake in the other tissues gradually decreased.

The effects of the co-injected unlabeled **1**, **2**, indomethacin or NS-398 on the tissue distribution of the two tracers at 30 min post injection are summarized in Tables 4 and 5. Carrier-loading and co-injection of non-selective indomethacin decreased the uptake of [^{11}C]**1** in the spleen and small intestine, lung (not significant in the case of indomethacin) and liver (not significant in the case of the carrier). Co-injection of **2** slightly reduced only the spleen uptake of [^{11}C]**1**. In the case of [^{11}C]**2**, carrier-loading significantly decreased the radioactivity levels in the spleen and blood, while none of the three other COX inhibitors showed blocking effects in any tissues but rather enhanced the radioactivity levels in a few tissues.

Metabolite analysis

By deproteinization with TCA/CH_3CN, most radioactivity (>97%) of the plasma and brain and AH109A tissues was recovered in the acid-soluble fractions in the metabolite analysis of [^{11}C]**2**, while the recovery was lower in the plasma (76%) and AH109A (93%) in the case of [^{11}C]**1**. The recovery of the radioactivity in the HPLC analysis was essentially quantitative in all cases. Although [^{11}C]**1** was less stable than [^{11}C]**2**, most radioactivity (>93%) of

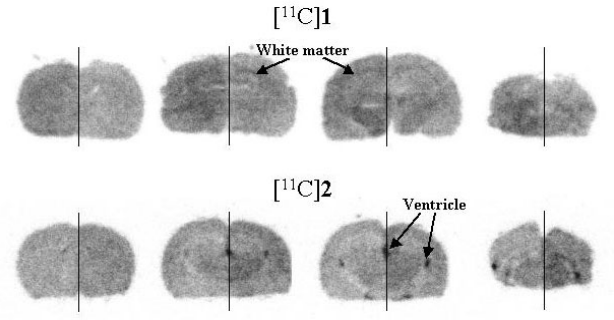

Fig. 2 *Ex vivo* autoradiograms of the brain sections 30 minutes after intravenous injection of [^{11}C]**1** (*upper*) and [^{11}C]**2** (*lower*) into rats. The left and right halves of each brain section show the control rat brain and the rat brain pretreated with indomethacin for [^{11}C]**1** or NS-398 for [^{11}C]**2**, respectively (n = 1 for each experiment). Apparent differences in the brain uptake of the two tracers between the control and drug-treated brains may be due to individual differences, because their distribution patterns were not changed, and because no statistical difference was found in the tissue distribution studies (Tables 4 and 5).

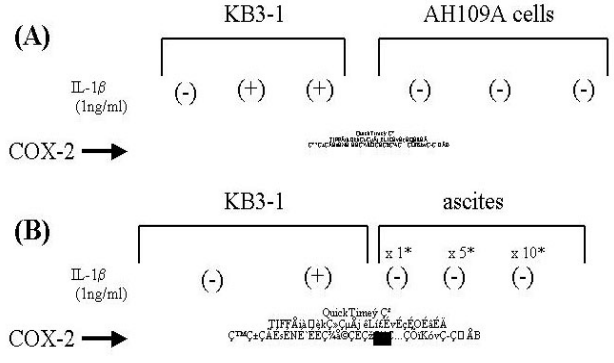

Fig. 3 Western blot analysis. (A), AH109A cells. (B), ascites of AH109A bearing Donryu rat. *Volume of protein compared to KB3-1.

the two tracers was detected as unchanged forms for both tracers in the brain and AH109A tissues.

Ex vivo autoradiographic study

In the *ex vivo* autoradiograms of control rat brain sections (Fig. 2), [^{11}C]**1** showed uniform distribution of the radioactivity with a slightly high density in the white matter, while [^{11}C]**2** showed regional differences with a high density in the ventricle. However, blocking effects of indomethacin for [^{11}C]**1** or NS-398 for [^{11}C]**2** were not clearly found.

In the *ex vivo* autoradiograms of AH109A sections, the distribution of the two tracers was not homogeneous in tissues (data not shown). No radioactivity was found in necrosis but a heterogeneous distribution was found, especially in [^{11}C]**2** sections with a large necrotic region.

COX-2 analysis

Western blot analysis (Fig. 3) showed that AH109H tumor cells expressed COX-2 protein.

DISCUSSION

We prepared two ^{11}C-labeled celecoxib derivatives [^{11}C]**1** and [^{11}C]**2** for mapping COX-1 and COX-2, respectively, by the *O*-[^{11}C]methylation method. The radiosynthesis was improved by the application of [^{11}C]methyl triflate as a labeling agent instead of [^{11}C]methyl iodide and the use of equimolar amount of base with respect to the phenolic precursors. It has been shown that [^{11}C]methyl triflate is a highly reactive alternative to [^{11}C]methyl iodide as a labeling agent, which offers an approach for an efficient labeling procedure.[33,36] This trend was also confirmed in our study.

COX-1 is highly expressed in the lung, liver, small intestine, spleen and kidney.[9,21] Compared with the peripheral tissues, COX-1 is poorly expressed in the brain, but distributed throughout the brain, most abundantly in the forebrain.[20] Although the accumulation of [^{11}C]**1** in these tissues was low, and the magnitude of uptake was similar to that in other tissues, co-injection of unlabeled **1** and a non-selective COX inhibitor, indomethacin, significantly decreased the uptake in the lung, small intestine and spleen. There is a tendency that the radioactivity is relatively retained in these tissues compared with other tissues. These findings seemingly suggest the minimal saturable or specific binding of [^{11}C]**1** to the COX-1 isozyme in these peripheral tissues. On the other hand, in the brain and AH109A hepatoma, the uptake was retained at low levels over 60 minutes, but no saturable or specific binding of [^{11}C]**1** to COX-1 was suggested in these tissues. COX-1 is poorly expressed in the brain[9] and it is unclear whether COX-1 was expressed in the AH109A.

In contrast to COX-1, COX-2 is predominantly expressed in the brain and to a lesser extent in the kidney, heart and lung.[9,21] In this study, only carrier-loading reduced the radioactivity levels in the spleen and blood but not in the brain and other tissues investigated. Although COX-2 is scarcely expressed in the spleen,[9] the presence of COXs in the blood cells is known.[3] Although we did not examine the uptake of [^{11}C]**2** in the blood cells, de Vries et al. demonstrated the specific binding of COX-2-selective [^{18}F]desbromo-DuP-697 to blood cells in a blocking study using NS-398 and indomethacin in rats.[27] In the brain, high basal levels of COX-2 were found in the hippocampus, cerebral cortex and amygdala complex.[37] Although the saturable or COX-specific binding of [^{11}C]**2** in the brain was not shown by the blocking study, the *ex vivo* brain autoradiogram of [^{11}C]**2** showed a distribution pattern similar to that of COXs, and also similar to that obtained by [^{18}F]desbromo-DuP-697. The blocking study was performed 30 min postinjection, because the radioactivity levels in the brain remained for 60 min. This

time point may not be suitable to detect a low level of the specific binding. The high radioactivity density of [^{11}C]**2** observed in the ventricle is probably due to a much higher blood level of [^{11}C]**2** compared with the brain uptake level. Brain uptake of [^{11}C]**2** was very low in spite of the reasonably high lipophilicity ($logP_{7.4}$ = 3.06) predicted for good brain entry. The reasons for this finding remain to be clarified but it may be the result of the phenomenon of blood-element binding by highly lipophilic [^{11}C]**2**.[3,24,38] In the blocking study using indomethacin, it is conceivable that the insensitivity of a blocking effect by administration of indomethacin may partly be due to the low penetration of indomethacin across the blood-brain barrier.[39] The *ex vivo* autoradiograms of [^{18}F]desbromo-DuP-697 showed COX-specific binding,[27] although it is a lower potent inhibitor of COX-2 with a higher lipophilicity. The other positron-emitting COX-2 inhibitor [^{18}F]SC58125 has a biodistribution compatible with the known distribution of the COX enzymes, but attempts to block tissue uptake were unsuccessful.[26] The IC_{50} value of [^{18}F]SC58125 (COX-2 IC_{50} < 86 nM)[26] is larger than that of [^{11}C]**2** (COX-2 IC_{50} = 8 nM)[24] but smaller than that of [^{18}F]desbromo-DuP-697 (COX-2 IC_{50} = 250 nM).[27,28]

Although we confirmed that the AH109A hepatoma cells and ascites of AH109A bearing rat are positive for COX-2, the absence of saturable or COX-specific binding of [^{11}C]**2** in the AH109A hepatoma was also suggested by the blocking experiments as shown in Table 5. However, *ex vivo* autoradiography showed regional differences in the distribution of [^{11}C]**2** in the AH109A section. The tissue dissection method used in the blocking study may not be suitable for evaluating specific binding of [^{11}C]**2** to COX-2 in high density regions if they have COX-2. Since a high percentage of both radiotracers after injection remained unchanged in AH109A and brain, it is suggested that the lack of blocking effects observed in these tissues is not simply due to the radiolabeled metabolites of the tracers.

The benzenesulfonamide moiety attached to the nitrogen atom of the pyrazole ring of celecoxib, belonging to the 1,5-diarylpyrazole class of inhibitors, is considered to be responsible for high potency and COX-2 selectivity.[40] Recently it has been demonstrated that COX-2-selective arylsulfonamide-type inhibitors show high affinity for carbonic anhydrase.[41] These indications suggest that cross-affinity with other enzymes, such as carbonic anhydrase, might contribute to increase the *in vivo* non-specific binding of [^{11}C]**2** containing a benzenesulfonamide group.

In conclusion, [^{11}C]**1** and [^{11}C]**2**, belong to the 1,5-diarylpyrazole class of compounds, reported to be selective inhibitors for COX-1 and COX-2 *in vitro*, respectively, were prepared by *O*-[^{11}C]methylation of the corresponding desmethyl precursors. *In vivo* evaluation in tumor-bearing rats showed only little evidence of specific binding of [^{11}C]**1** to COX-1 in peripheral organs. Carrier-saturable uptake of [^{11}C]**2** was found in the spleen. The blocking study, however, did not support COX-specific binding of [^{11}C]**2**. The result suggests that neither [^{11}C]**1** nor [^{11}C]**2** is a suitable tracer for *in vivo* mapping of COX-1 and COX-2 isoforms. Analogs of higher binding affinity may be required for *in vivo* imaging of COX enzymes with this class of compounds.

REFERENCES

1. Smith WL, Marnett LJ, Dewitt DL. Prostaglandin and thromboxane biosynthesis. *Pharmacol Ther* 1991; 49: 153–179.
2. Xie W, Chipman JG, Robertson DL, Erikson RL, Simmons DL. Expression of a mitogen-responsive gene encoding prostaglandin synthase is regulated by mRNA splicing. *Proc Natl Acad Sci USA* 1991; 88: 2692–2696.
3. Fu JY, Masferrer JL, Seibert K, Raz A, Needleman P. The induction and suppression of prostaglandin H2 synthase (cyclooxygenase) in human monocytes. *J Biol Chem* 1990; 265: 16737–16740.
4. Kujubu DA, Fletcher BS, Varnum BC, Lim RW, Herschman HR. TIS10, a phorbol ester tumor promoter-inducible mRNA from Swiss 3T3 cells, encodes a novel prostaglandin synthase/cyclooxygenase homologue. *J Biol Chem* 1991; 266: 12866–12872.
5. Hla T, Neilson K. Human cyclooxygenase-2 cDNA. *Proc Natl Acad Sci USA* 1992; 89: 7384–7388.
6. Goppelt-Struebe M. Regulation of prostaglandin endoperoxide synthase (cyclooxygenase) isozyme expression. *Prostaglandins Leukot Essent Fatty Acids* 1995; 52: 213–222.
7. Futaki N, Takahashi S, Yokoyama M, Arai I, Higuchi S, Otomo S. NS-398, a new anti-inflammatory agent, selectively inhibits prostaglandin G/H synthase/cyclooxygenase (COX-2) activity *in vitro*. *Prostaglandins* 1994; 47: 55–59.
8. Copeland RA, Williams JM, Giannaras J, Nurnberg S, Covington M, Pinto D, et al. Mechanism of selective inhibition of the inducible isoform of prostaglandin G/H synthase. *Proc Natl Acad Sci USA* 1994; 91: 11202–11206.
9. Seibert K, Zhang Y, Leahy K, Hauser S, Masferrer J, Perkins W, et al. Pharmacological and biochemical demonstration of the role of cyclooxygenase 2 in inflammation and pain. *Proc Natl Acad Sci USA* 1994; 91: 12013–12017.
10. Eberhart CE, Coffey RJ, Radhika A, Giardiello FM, Ferrenbach S, DuBois RN. Up-regulation of cyclooxygenase 2 gene expression in human colorectal adenomas and adenocarcinomas. *Gastroenterology* 1994; 107: 1183–1188.
11. Sano H, Kawahito Y, Wilder RL, Hashiramoto A, Mukai S, Asai K, et al. Expression of cyclooxygenase-1 and -2 in human colorectal cancer. *Cancer Res* 1995; 55: 3785–3789.
12. Kutchera W, Jones DA, Matsunami N, Groden J, McIntyre TM, Zimmerman GA, et al. Prostaglandin H synthase 2 is expressed abnormally in human colon cancer: evidence for a transcriptional effect. *Proc Natl Acad Sci USA* 1996; 93: 4816–4820.
13. Wolff H, Saukkonen K, Anttila S, Karjalainen A, Vainio H, Ristmaki A. Expression of cyclooxygenase-2 in human lung carcinoma. *Cancer Res* 1998; 58: 4997–5001.
14. Hida T, Yatabe Y, Achiwa H, Muramatsu H, Kozaki K, Nakamura S, et al. Increased expression of cyclooxygenase

2 occurs frequently in human lung cancers, specifically in adenocarcinomas. *Cancer Res* 1998; 58: 3761–3764.
15. Subbaramaiah K, Telang N, Ramonetti JT, Araki R, DeVito B, Weksler BB, et al. Transcription of cyclooxygenase-2 is enhanced in transformed mammary epithelial cells. *Cancer Res* 1996; 56: 4424–4429.
16. Subbaramaiah K, Dannenberg AJ. Cyclooxygenase 2: a molecular target for cancer prevention and treatment. *Trends Pharmacol Sci* 2003; 24: 96–102.
17. Evans JF, Kargman SL. Cancer and cyclooxygenase-2 (COX-2) inhibition. *Curr Pharm Des* 2004; 10: 627–634.
18. Kaufmann WE, Andreasson KI, Isakson PC, Worley PF. Cyclooxygenases and the central nervous system. *Prostaglandins* 1997; 54: 601–624.
19. Yermakova A, O'Banion MK. Cyclooxygenases in the central nervous system: implications for treatment of neurological disorders. *Curr Pharm Des* 2000; 6: 1755–1776.
20. Kam PCA, See AUL. Cyclo-oxygenase isoenzymes: physiological and pharmacological role. *Anaesthesia* 2000; 55: 442–449.
21. Okamoto T, Hino O. Expression of cyclooxygenase-1 and -2 mRNA in rat tissues: tissue-specific difference in the expression of the basal level of mRNA. *Int J Mol Med* 2000; 6: 455–457.
22. Yamagata K, Andreasson KI, Kaufman WE, Barnes CA, Worsley PF. Expression of a mitogen-inducible cyclooxygenase in brain neurons. *Neuron* 1993; 11: 371–386.
23. Holtz ML, Kindy MS, Craddock S, Moore RW, Pettigrew LC. Induction of PGH synthase and c-*fos* mRNA during early reperfusion of ischemic rat brain. *Mol Brain Res* 1996; 35: 339–343.
24. Penning TD, Talley JJ, Bertenshaw SR, Carter JS, Collins PW, Docter S, et al. Synthesis and biological evaluation of the 1,5-diarylpyrazole class of cyclooxygenase-2 inhibitors: identification of 4-[5-(4-methylphenyl)-3-(trifluoromethyl)-1*H*-pyrazol-1-yl]benzenesulfonamide (SC-58635, celecoxib). *J Med Chem* 1997; 40: 1347–1365.
25. Prasit P, Wang Z, Brideau C, Chan CC, Charleson S, Cromlish W, et al. The discovery of rofecoxib, [MK 966, VIOXX, 4-(4′-methylsulfonylphenyl)-3-phenyl-2(5*H*)-furanone], an orally active cyclooxygenase-2 inhibitor. *Bioorg Med Chem Lett* 1999; 9: 1773–1778.
26. McCarthy TJ, Sheriff AU, Graneto MJ, Talley JJ, Welch MJ. Radiosynthesis, *in vitro* validation, and *in vivo* evaluation of ^{18}F-labeled COX-1 and COX-2 inhibitors. *J Nucl Med* 2002; 43: 117–124.
27. de Vries EFJ, van Waarde A, Buursma AR, Vaalburg W. Synthesis and *in vivo* evaluation of ^{18}F-desbromo-Dup-697 as a PET tracer for cyclooxygenase-2 expression. *J Nucl Med* 2003; 44: 1700–1706.
28. Leblanc Y, Gauthier JY, Ethier D, Guay J, Mancini J, Riendeau D, et al. Synthesis and biological evaluation of 2,3-diarylthiophenes as selective COX-2 and COX-1 inhibitors. *Bioorg Med Chem Lett* 1995; 5: 2123–2128.
29. Smith CJ, Zhang Y, Koboldt CM, Muhammad J, Zweifel BS, Shaffer A, et al. Pharmacological analysis of cyclooxygenase-1 in inflammation. *Proc Natl Acad Sci USA* 1998; 95: 13313–13318.
30. Tanaka A, Hase S, Miyazawa T, Takeuchi K. Up-regulation of cyclooxygenase-2 by inhibition of cyclooxygenase-1: a key to nonsteroidal anti-inflammatory drug-induced intestinal damage. *J Pharmacol Exp Ther* 2002; 300: 754–761.
31. Ishiwata K, Kawamura K, Wang WF, Furumoto S, Kubota K, Pascali C, et al. Evaluation of *O*-[^{11}C]methyl-L-tyrosine and *O*-[^{18}F]fluoromethyl-L-tyrosine as tumor imaging tracers by PET. *Nucl Med Biol* 2004; 31: 191–198.
32. Ishiwata K, Seki H, Ishii K, Ishii S, Nozaki T, Senda M. Synthesis and *in vivo* evaluation of [^{11}C]semotiadil, a benzothiazine calcium antagonist. *Appl Radiat Isot* 1994; 45: 439–443.
33. Kawamura K, Ishiwata K. Improved synthesis of [^{11}C]SA4503, [^{11}C]MPDX and [^{11}C]TMSX by use of [^{11}C]methyl triflate. *Ann Nucl Med* 2004; 18: 165–168.
34. Gierse JK, Hauser SD, Creely DP, Koboldt C, Rangwala SH, Isakson PC, et al. Expression and selective inhibition of the constitutive and inducible forms of human cyclo-oxygenase. *Biochem J* 1995; 305: 479–484.
35. Hirata A, Hosoi F, Miyagawa M, Ueda S, Naito S, Fujii T, et al. HER2 overexpression increases sensitivity to Gefitinib, an epidermal growth factor receptor tyrosine kinase inhibitor, through inhibition of HER2/HER3 heterodimer formation in lung cancer cells. *Cancer Res* 2005; 65: 4253–4260.
36. Någren K, Halldin C. Methylation of amide and thiol functions with [^{11}C]methyl triflate, as exemplified by [^{11}C]NMSP, [^{11}C]flumazenil and [^{11}C]methionine. *J Label Compd Radiopharm* 1998; 41: 831–841.
37. Breder CD, Dewitt D, Kraig RP. Characterization of inducible cyclooxygenase in rat brain. *J Comp Neurol* 1995; 355: 296–315.
38. Paulson SK, Kaprak TA, Gresk CJ, Fast DM, Baratta MT, Burton EG, et al. Plasma protein binding of celecoxib in mice, rat, rabbit, dog and human. *Biopharm Drug Dispos* 1999; 20: 293–299.
39. Clark DE. *In silico* prediction of blood-brain barrier permeation. *Drug Discov Today* 2003; 8: 927–933.
40. Kurumbail RG, Stevens AM, Gierse JK, McDonald JJ, Stegeman RA, Pak JY, et al. Structural basis for selective inhibition of cyclooxygenase-2 by anti-inflammatory agents. *Nature* 1996; 384: 644–648.
41. Weber A, Casini A, Heine A, Kuhn D, Supuran CT, Scozzafava A, et al. Unexpected nanomolar inhibition of carbonic anhydrase by COX-2-selective celecoxib: new pharmacological opportunities due to related binding site recognition. *J Med Chem* 2004; 47: 550–557.